



## Dinitrogen Activation Hot Paper

How to cite: *Angew. Chem. Int. Ed.* **2021**, *60*, 17205–17210

International Edition: doi.org/10.1002/anie.202106984

German Edition: doi.org/10.1002/ange.202106984

# Cleavage of the N≡N Triple Bond and Unpredicted Formation of the Cyclic 1,3-Diaza-2,4-Diborete (FB)<sub>2</sub>N<sub>2</sub> from N<sub>2</sub> and Fluoroborylene BF

Bing Xu, Helmut Beckers, Haoyu Ye, Yan Lu, Juanjuan Cheng, Xuefeng Wang,\* and Sebastian Riedel\*

Dedicated to Professor Hansgeorg Schnöckel on the occasion of his 80<sup>th</sup> birthday

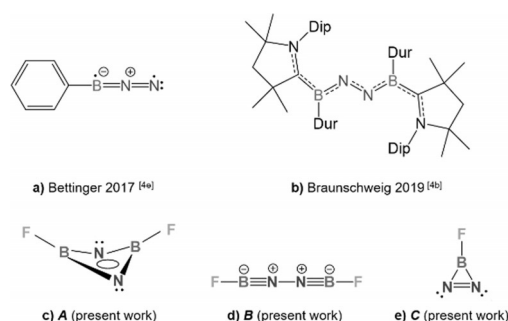
**Abstract:** A complete cleavage of the triple bond of N<sub>2</sub> by fluoroborylene (:BF) was achieved in a low-temperature N<sub>2</sub> matrix by the formation of the four-membered heterocycle FB(μ-N)<sub>2</sub>BF, which lacks a trans-annular N–N bond. Additionally, the linear complex FB=N–N=BF and cyclic FB(η<sup>2</sup>-N<sub>2</sub>) were formed. These novel species were characterized by their matrix infrared spectra and quantum-chemical calculations. The puckered four-membered-ring B<sub>2</sub>N<sub>2</sub> complex shows a delocalized aromatic two-electron π-system in conjugation with the exo-cyclic fluorine π lone pairs. This work may contribute to a rational design of catalysts based on borylene for artificial dinitrogen activation.

## Introduction

The cleavage of the N≡N triple bond (one of the strongest chemical bond) is a long-standing task in chemistry.<sup>[1]</sup> Since the discovery of the Haber-Bosch process for producing ammonia from H<sub>2</sub>/N<sub>2</sub> in the first decade of the 20<sup>th</sup> century, plenty of transition-metal (TM) complexes have been discovered to activate and functionalize thermodynamically stable and kinetically inert dinitrogen (N<sub>2</sub>) under more ambient conditions.<sup>[2]</sup> For *p*-block elements the examples of N<sub>2</sub> binding are mainly contributed from boron compounds such as borylenes (:BR).<sup>[3]</sup> The boron atom in borylene possess both, a lone pair of electrons (HOMO) and an energetically low-lying empty *p* valence orbital (LUMO). Borylenes are therefore excellent candidate for mimicking transition-metal reactivity.<sup>[4]</sup> The reaction of N<sub>2</sub> with free

phenylborylene, :BPh, under matrix conditions has been shown to yield the linear adduct PhB=NN in a triplet ground state, underscoring the use of borylenes as candidates for N<sub>2</sub> binding (Scheme 1 a).<sup>[4e]</sup> A boron-based fixation of N<sub>2</sub> has very recently also been reported using a phenylborylene stabilized by a bulky carbene ligand, [(CAAC)DurB] (CAAC = cyclic alkylamino carbene, Dur = 2,3,5,6-tetramethylphenyl), leading to the end-on bridging complex [(CAAC)DurB]<sub>2</sub>(μ<sup>2</sup>-N<sub>2</sub>)<sup>[4b]</sup> in which the N–N bond length [1.248(4) Å] lies in the range of N=N double bonds (Scheme 1 b).<sup>[5]</sup>

The reaction of laser-ablated boron atoms with N<sub>2</sub> molecules upon co-deposition onto a cooled (4 K) CsI window has previously been studied.<sup>[6]</sup> These studies provided a variety of mono and diboron nitrogen compounds of the type BN<sub>2</sub>, B<sub>2</sub>N, and B<sub>2</sub>N<sub>2</sub> as well as linear NNBN.<sup>[6]</sup> It has recently been shown, that addition of CO to the boron-N<sub>2</sub> deposits gives rise to CO complexes of the BN<sub>2</sub> isomers, such as the chain-molecules NNBCO and NBNCO, cyclic (η<sup>2</sup>-N<sub>2</sub>)BCO, and the diisocyanat B(NCO)<sub>2</sub>.<sup>[7]</sup>



**Scheme 1.** Five different binding modes of N<sub>2</sub> to borylenes.

## Results and Discussion

Here we report on novel fluoroborylene (:BF) : N<sub>2</sub> compounds, the cyclic diaza-diborete FB(μ-N)<sub>2</sub>BF (**A**), its linear FB=N–N=BF isomer (**B**), and cyclic fluorodiazaboririne, FB(η<sup>2</sup>-N<sub>2</sub>) (**C**) which was previously predicted<sup>[8]</sup> (Scheme 1, c–e). They are selectively formed upon co-deposition of laser-ablated boron atoms with elemental fluorine in an N<sub>2</sub> gas stream at cryogenic temperatures (4 ± 1 K, for experimental details see the Supporting Information). Here, dinitrogen molecules act as both, reactants and host matrix. The cyclic compounds **A** and **C** are of aromatic

[\*] Prof. Dr. B. Xu, H. Ye, J. Cheng, Prof. Dr. X. Wang  
School of Chemical Science and Engineering Department, Shanghai  
Key lab of Chemical Assessment and Sustainability, Tongji University  
Shanghai, 200092 (China)  
E-mail: xfwang@tongji.edu.cn  
Prof. Dr. B. Xu, Dr. H. Beckers, Y. Lu, Prof. Dr. S. Riedel  
Institut für Chemie und Biochemie – Anorganische Chemie, Freie  
Universität Berlin  
Fabeckstrasse 34–36, 14195 Berlin (Germany)  
E-mail: s.riedel@fu-berlin.de

Supporting information and the ORCID identification number(s) for the author(s) of this article can be found under:  
https://doi.org/10.1002/anie.202106984.

© 2021 The Authors. Angewandte Chemie International Edition published by Wiley-VCH GmbH. This is an open access article under the terms of the Creative Commons Attribution License, which permits use, distribution and reproduction in any medium, provided the original work is properly cited.

nature due to the presence of a delocalized  $2\pi$  electron bond which is in conjugation with the  $\pi$  lone pairs of the *exo*-cyclic F atoms indicating a type of fluorine specific interactions.

Figure 1 shows infrared spectra obtained after laser-ablated natural boron atoms co-deposited with a 0.5%  $F_2/N_2$  mixture in a 4 K dinitrogen matrix. The reaction products induced by annealing and photolysis are indicated. In addition to the three novel fluoroborylene :  $N_2$  products **A–C** binary boron fluorides  $BF_n$  ( $n=1-3$ ) and the molecular boron nitrides NBN and NNBN<sup>[6]</sup> were obtained in the present study, while the previously reported diboron compounds BBNN and BNNB<sup>[6]</sup> were barely observed (Figure 1 and Table S1). Although  $BF_2$  and  $BF_3$  are also produced,<sup>[9]</sup> the reaction conditions were optimized to achieve a maximum yield of fluoroborylene, BF (see experimental details in the Supporting Information). The strong bands for  $^{11}BF$  and  $^{10}BF$  were found at 1370.6 and 1412.4  $cm^{-1}$ , respectively (Figure 1, Table S2). These optimized conditions enabled us to tentatively assign three weak bands to different  $^{10/11}B$  isotopologues of difluorodiborene, FBBF, at 1327.3 ( $^{11}B^{11}B$ ), 1348.5 ( $^{10}B^{11}B$ ) and 1370.3  $cm^{-1}$  ( $^{10}B^{10}B$ ) in experiments using a natural boron target in  $N_2$  and  $^{15}N_2$  matrices (Figure 1 and S3). Owing to its high reactivity, experimental spectra of free FBBF have not yet been reported, although complexes of FBBF with electron-rich transition metals have been investigated.<sup>[10]</sup>

The absorptions associated with the novel fluoroborylene :  $N_2$  product molecules **A–C** were unambiguously assigned based on their growth/decay characteristics in different experiments and on their characteristic  $^{10/11}B$  and  $^{14/15}N$  isotope pattern. The novel ring molecule **A** shows strong bands in the B-F stretching region at 1531.0 and 1558.6  $cm^{-1}$ , which are tracked by weaker ring vibrations at 1090.7 and 1101.5  $cm^{-1}$ . These bands were already observed on deposition, they increased by 50% on annealing to 15 K, and

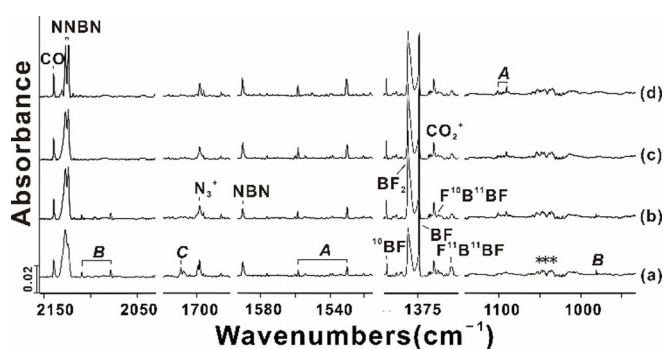


**Figure 1.** Excerpts from the IR spectrum obtained using a natural boron target with 0.5%  $F_2$  in  $N_2$  matrix: (a) co-deposition of B + 0.5%  $F_2$  for 120 min, (b) after annealing to 15 K, (c) after subsequent  $\lambda = 273$  nm irradiation for 30 min, and (d) further annealing to 15 K. Unknown species are indicated by asterisks.

continue to grow on irradiation at  $\lambda = 278 \pm 10$  nm, where they reached three-fold on further annealing to 15 K. For a natural boron ( $^{10}B:^{11}B = 19.9:80.1$ ) sample, the vibrational modes of a diboron species with two equivalent boron atoms split into three absorptions with approximately 1:8:16 ( $^{10}B^{10}B$ ,  $^{10}B^{11}B$ ,  $^{11}B^{11}B$ ) relative intensities.<sup>[11]</sup> In addition to the two B-F stretching bands for the two most abundant isotopologues of **A** (Tables 1 and S3) the corresponding band associated with the  $^{10}B^{10}B$  species is observed in  $^{10}B + F_2/N_2$  mixture experiments at 1590.2  $cm^{-1}$ , giving a  $^{10}B^{11}B$  isotopic ratio of 1.0381. The  $^{11}B^{11}B$  ring vibration observed at 1090.7  $cm^{-1}$  shift to 1123.8  $cm^{-1}$  ( $^{10}B^{10}B$ ) in these experiments, indicating a  $^{10}B/^{11}B$  isotopic ratio of 1.0303, a typical boron atom involved isotopic ratio. As shown in Figure 2 the boron isotopic distribution supports the presence of two equivalent boron atoms in this molecule. In experiments using  $F_2/^{15}N_2$  mixtures

**Table 1:** Observed and calculated (CCSD(T)/def2-TZVP) vibrational frequencies ( $cm^{-1}$ ) and isotopic frequency ratios ( $\nu(^{10}B)/\nu(^{11}B)$ ) of the  $FB(\mu-N)_2BF$ ,  $FBNNBF$  and  $FB(\eta^2-N_2)$  molecules.<sup>[a]</sup>

	$^{11}B^{11}B/^{11}B$		$^{10}B^{11}B$		$^{10}B^{10}B/^{10}B$		$^{10}B/^{11}B$ ratio	
	calcd <sup>[a]</sup>	Obs.	calcd <sup>[a]</sup>	Obs.	calcd <sup>[a]</sup>	Obs.	calcd	Obs.
cyclic $FB(\mu-N)_2BF$ ( $^1A_1$ )								
	1612.7 (68)	1612.8	1642.2 (88)	1635.8	1662.9 (70)	1660.7	1.0311	1.0297
$^{14}N$	1538.5 (802)	1531.0	1546.2 (733)	1558.6	1585.1 (850)	1590.2	1.0302	1.0382
	1114.6 (113)	1090.7	1125.4 (115)	1101.5	1140.5 (120)	1123.8	1.0232	1.0303
	1597.1 (57)	hidden	1638.2 (87)	/	1659.2 (64)	1662.8	1.0387	/
$^{15}N$	1523.2 (785)	1521.4	1541.8 (727)	1542.0	1580.1 (844)	1569.6	1.0377	1.0317
	1093.5 (110)	1077.0	1110.5 (113)	/	1125.8 (118)	1108.5	1.0295	1.0292
linear $FBNNBF$ ( $^1\Sigma_g^+$ )								
$^{14}N$	2068.8 (927)	2078.2	2099.0 (934)	2108.8	2138.6 (1012)	2147.0	1.0337	1.0331
	976.1 (178)	981.0	977.4 (176)	/	978.9 (174)	983.1	1.0029	1.0021
$^{15}N$	2049.5 (933)	hidden	2079.2 (929)	2073.4	2120.2 (1017)	2125.0	1.0345	/
	962.7 (168)	969.4	963.8 (166)	/	964.9 (165)	970.4	1.0023	1.0010
cyclic $FB(\eta^2-N_2)$ ( $^1A_1$ )								
$^{14}N$	1704.5 (356)	1710.5			1760.6 (355)	1765.8	1.0330	1.0323
	1231.6 (45)	1229.5			1234.9 (46)	1231.0	1.0027	1.0012
$^{15}N$	1689.6 (398)	1700.1			1752.3 (340)	/	1.0371	/
	1194.8 (35)	1192.5			1198.6 (33)	/	1.0032	/

[a] Scaled frequencies using a uniform scaling factor of 0.969.<sup>[27]</sup> Intensities ( $km\ mol^{-1}$ ) in parentheses. Band positions assigned to B-F stretching modes are given in italics.

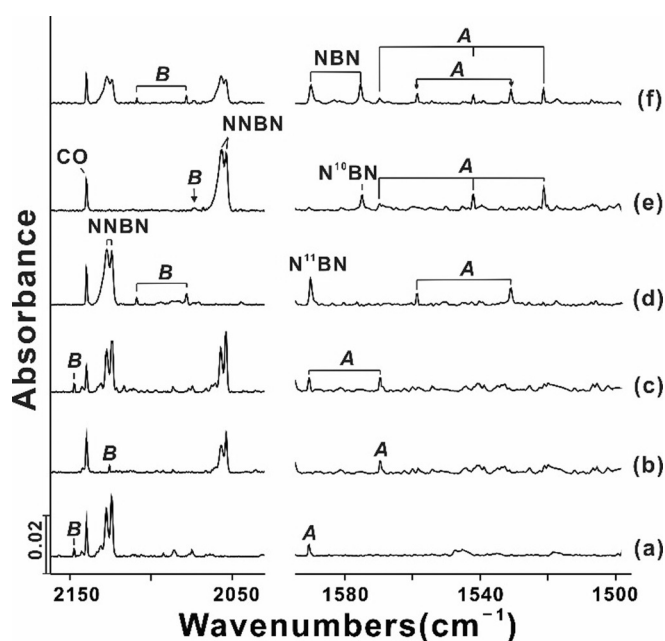


**Figure 2.** Excerpts from the IR spectrum obtained using a  $^{10}\text{B}$  target with 0.5%  $\text{F}_2$  in (a)  $^{14}\text{N}_2$  matrix, (b)  $^{15}\text{N}_2$  matrix, and (c) 50%  $^{14}\text{N}_2$  + 50%  $^{15}\text{N}_2$  matrix. Natural boron target with 0.5%  $\text{F}_2$  in (d)  $^{14}\text{N}_2$  matrix, (e)  $^{15}\text{N}_2$  matrix, and (f) 50%  $^{14}\text{N}_2$  + 50%  $^{15}\text{N}_2$  matrix.

(Figure 2) the  $^{15}\text{N}$  counterpart bands were observed at 1569.6 and 1108.5  $\text{cm}^{-1}$  ( $^{10}\text{B}^{10}\text{B}$ ), 1542.0  $\text{cm}^{-1}$  ( $^{10}\text{B}^{11}\text{B}$ ) and 1521.4 and 1077.0  $\text{cm}^{-1}$  ( $^{11}\text{B}^{11}\text{B}$ ), respectively (Figures S1). The relative intensities of the bands due to the  $^{14}\text{N}$  and  $^{15}\text{N}$  isotopomers are almost the same in experiments using 50%  $^{14}\text{N}_2$  and 50%  $^{15}\text{N}_2$  mixtures (Figure 2f). Obviously, two B atoms bind only one  $^{14}\text{N}_2$  or  $^{15}\text{N}_2$  in this new ring molecule. We also note a good agreement between the observed and calculated frequencies at the B3LYP and CCSD(T) levels of theory listed in Tables 1 and S3.

The linear isomer **B** ( $D_{\infty h}$  symmetry, Figure 3) has a singlet ground state and exhibits only two infrared active vibrational modes in the mid-IR region (Table S4, for more computa-

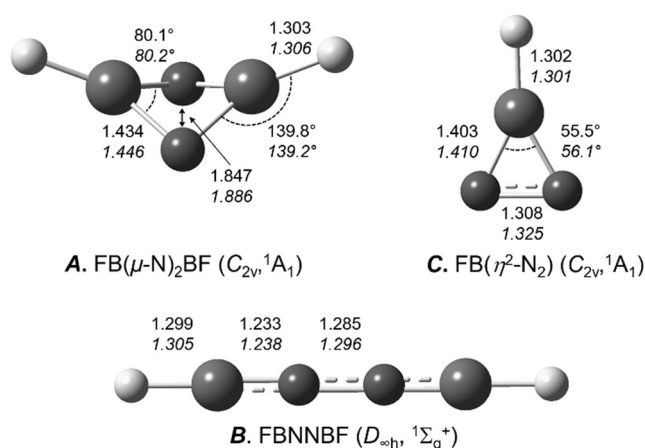


**Figure 3.** Optimized structures of **A**  $\text{FB}(\mu\text{-N})_2\text{BF}$ , **B**  $\text{FBNNBF}$  and **C**  $\text{FB}(\eta^2\text{-N}_2)$  (NN) obtained at the B3LYP/6-311++G(3df,3pd) and CCSD(T)/def2-TZVP (*italic*) levels of theory. Bond distances are given in Å and angles in degree.

tional results on **B** see Part 1 of the Supporting Information). The antisymmetric B-N stretching modes give rise to two bands at 2108.8 ( $^{11}\text{B}^{10}\text{B}$ ) and 2078.2 ( $^{11}\text{B}^{11}\text{B}$ )  $\text{cm}^{-1}$  in Figure 1 using a natural boron target, while the antisymmetric F-B vibration is observed only for the most abundant  $^{11}\text{B}^{11}\text{B}$  isotopologue at 981.0  $\text{cm}^{-1}$  on deposition. Experiments performed with  $^{10}\text{B}$  and  $\text{N}_2$  or  $^{15}\text{N}_2$ , and  $^{11}\text{B}$  with  $\text{N}_2$  or  $^{15}\text{N}_2$  are shown in Figures 2 and S1–S3, and the observed product absorptions are compared to calculated values in Table 1 (for more details see the Supporting Information). These bands disappeared upon 273 nm irradiation, while the bands of **A** increased simultaneously, suggesting that isomerization is occurring. Note, linear **B** is isoelectronic to diisocyanate,  $\text{OCNNCO}$ .<sup>[12]</sup> Like **B** also  $\text{OCNNCO}$  is photosensitive and decomposes rapidly under UV light to produce  $\text{N}_2 + 2 \text{CO}$ .

Cyclic **C** (Figure 3) is assigned to a band at 1710.5  $\text{cm}^{-1}$  in Figure 1, and another very small band at 1229.5  $\text{cm}^{-1}$ , which corresponds to the F-B and N-N stretching modes, respectively (Tables 1 and S5). Further experiments were performed using  $^{10}\text{B}$  and  $\text{N}_2$  or  $^{15}\text{N}_2$ , and  $^{11}\text{B}$  with  $\text{N}_2$  or  $^{15}\text{N}_2$ , and the absorptions of the corresponding isotopologues were observed at 1765.8 and 1331.0  $\text{cm}^{-1}$  ( $^{10}\text{B}$ ), and at 1700.1 and 1192.5  $\text{cm}^{-1}$  ( $^{15}\text{N}$ , Figures S1,S3). These bands were observed on co-deposition, but on annealing to 15 K they disappeared entirely, while the bands due to **A** increased by 30%.

According to B3LYP/6-311++G(3df,3pd) calculation linear **B** is separated from cyclic **A** by a barrier of 25.0  $\text{kcal mol}^{-1}$  and higher in energy by 22.3  $\text{kcal mol}^{-1}$  (Figures S5, S11). At this level the predicted N-N distance in **A** is 1.847 Å (CCSD(T)/def2-TZVP: 1.886 Å), which is significantly longer than for example, the N-N single bond of diphenylhydrazine [ $d(\text{N-N})$ : 1.394 Å]<sup>[5]</sup> and indicates a complete splitting of the  $\text{N}\equiv\text{N}$  triple bond by the two FB units. The computed B-N distance (1.434 Å, Figure 3) is in the range of a conventional B=N double bond, like in aminoboranes.<sup>[13]</sup> The ring inversion barrier of the puckered ring of **A** was found to be 15.8  $\text{kcal mol}^{-1}$  at the B3LYP/6-311++G(3df,3pd) level of theory (Figure S13).

The proposed aromatic  $\pi$ -electron delocalization in the cyclic compounds **A** and **C** is supported by a molecular orbital (MO) analysis and computed nucleus-independent chemical shift (NICS) values. Figures 4 and S14 shows typical  $\pi$ -bonding orbitals of the cyclic  $\pi$ -conjugated system **A**, which consists of the 4c-2e central bonding orbital (HOMO-2) and two further  $\pi$ -bonding orbitals (HOMO-6 and -7), to which the exo-cyclic F atoms clearly contribute. Related puckered 4-membered ring aromates have previously thoroughly been analyzed.<sup>[14,15]</sup>

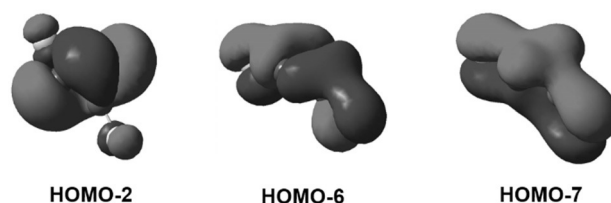


**Figure 4.** Selected frontier molecular orbitals of  $\text{FB}(\mu\text{-N})_2\text{BF}$ .

The NICS value is among the most popular aromaticity indices.<sup>[16]</sup> While the NICS index was originally obtained for planar aromatic systems, it has recently been suggested to calculate an average NICS(1)<sub>av</sub> index,  $\text{NICS}(1)_{\text{av}} = [\text{NICS}(-1) + \text{NICS}(1)]/2$ , as a probe of aromaticity in nonplanar molecular systems.<sup>[17]</sup> The large negative NICS(1)<sub>av</sub> index of  $-21$  obtained at the center of gravity of **A** (Figure S15,b) indicates its significant aromatic character, which can be compared to the NICS(1) value obtained for planar **C** of  $-12$  (Figure S15 e).

The selective formation of the products **A–C** is surprising at first glance, but due to a high dilution of the initially formed reactive intermediates, as well as the subsequent isolation of the products in a solid N<sub>2</sub> matrix at cryogenic temperatures, possible secondary reactions are efficiently suppressed. The predominant reaction of laser ablated boron atoms with N<sub>2</sub> molecules<sup>[6]</sup> depends on whether the boron atoms are in their <sup>2</sup>P(2s<sup>2</sup>2p<sup>1</sup>) or first excited <sup>4</sup>P(2s<sup>1</sup>2p<sup>2</sup>) state, located 82.5 kcal mol<sup>-1</sup> higher in energy.<sup>[18]</sup> Common trivalent boron compounds can usually be traced back to the first excited <sup>4</sup>P state, and sub-valent boron compounds such as Lewis-base stabilized borylenes only recently became a rapidly emerging class of highly reactive intermediates.<sup>[3,4]</sup> However, due to the very low Lewis basicity of N<sub>2</sub> it seems that ground-state boron atoms are reluctant to react with N<sub>2</sub> molecules.<sup>[6,19a]</sup> The dissociation energy of the weakly bound B-NN (<sup>2</sup>Π) adduct with respect to B(<sup>2</sup>P) + N<sub>2</sub> (<sup>X</sup>1Σ<sub>g</sub><sup>+</sup>) is reported to be only 1.2 kcal mol<sup>-1</sup>.<sup>[20]</sup> It is interesting that only the high-energy isomer NBN (<sup>2</sup>Π) is observed in the present study (Figures 1, 2). The weakly bound B-NN (<sup>2</sup>Π) adduct is almost isoenergetic with the cyclic isomer B(η<sup>2</sup>-N<sub>2</sub>) (<sup>2</sup>A<sub>1</sub>), while the linear trivalent boron isomers BNN (<sup>4</sup>Σ<sub>g</sub><sup>-</sup>) and NBN (<sup>2</sup>Π) are substantially higher in energy by 7.7 and 22 kcal mol<sup>-1</sup>, respectively.<sup>[20]</sup> Given that the adduct B-NN (<sup>2</sup>Π) is separated from the other three isomers by significant computed energy barriers,<sup>[19b]</sup> the observation of only the highest-energy isomer NBN (<sup>2</sup>Π) could indicate its higher kinetic stability compared to the other isomers under the experimental conditions. A plausible route to the formation of NBN is the reaction of N<sub>2</sub> molecules upon the deposition with excited <sup>4</sup>P boron atoms, which are produced during laser-ablation.

Prominent bands due to NNBN (<sup>1</sup>Σ<sub>g</sub><sup>+</sup>) and BF (<sup>1</sup>Σ<sub>g</sub><sup>+</sup>) in the spectra obtained after deposition (Figure 1) indicates the presence of free N and F atoms in the deposit. These atoms are commonly generated in the hot plasma plume or by photo-decomposition of N<sub>2</sub> and F<sub>2</sub> molecules, respectively, as a result of the plasma broadband radiation that is produced during laser ablation. These atoms react very exothermically with boron atoms to yield diatomic NB and FB molecules, respectively, but only NB react further with N<sub>2</sub> molecules during deposition to yield NNBN.<sup>[6]</sup> In addition, the lack of mixed <sup>14</sup>N/<sup>15</sup>N isotopologues of NBN in experiments using 1:1 mixtures of <sup>14</sup>N<sub>2</sub> and <sup>15</sup>N<sub>2</sub> rule out the formation of NBN from diatomic BN and N atoms, which corroborates our assumption of NBN formation by insertion of excited B atoms into N<sub>2</sub> molecules.

Our search for FBNN (Figure S19) in the experimental spectra failed, and, in contrast to NNBN and PhB-NN<sup>[4c]</sup> free diatomic BF was observed. In agreement with previous

results<sup>[8]</sup> our calculations revealed that the linear adduct FBNN is endothermic by 23.4 kcal mol<sup>-1</sup> compared to N<sub>2</sub> + singlet FB (Figure S19). This observation is consistent with the larger singlet-triplet gap of FB (+80 kcal mol<sup>-1</sup>)<sup>[20a]</sup> compared to that of diatomic NB ( $-0.5$  kcal mol<sup>-1</sup>)<sup>[20b]</sup> and PhB (+31 kcal mol<sup>-1</sup>).<sup>[20c]</sup>

For the formation of the novel FB : N<sub>2</sub> adducts **A–C**, we have explored both the fluorination of initially formed BN<sub>2</sub> intermediates and the reaction of fluoroborylene FB with N<sub>2</sub> molecules (Figures S4, S5). Although the reaction of the BN<sub>2</sub> species with F atoms is strongly exothermic, preliminary B3LYP/6-311 ++ G(3df,3pd) calculations suggest significant reaction barriers, for example, 14 kcal mol<sup>-1</sup> for the reaction of NBN (<sup>2</sup>Π) with F atoms (Figure S4). These calculations also revealed that cyclic **C** is higher in energy by 8.1 kcal mol<sup>-1</sup>, but kinetically stable to its decomposition into N<sub>2</sub> + singlet FB due to a barrier of 42 kcal mol<sup>-1</sup> (Figure S5).

Activation of N<sub>2</sub> molecules and weakening of its π bonds can mainly be attributed to interactions that donate electron density to its π\* antibonding orbitals, and remove electron density from the π bonding orbitals of N<sub>2</sub>.<sup>[21]</sup> Unlike transition metal complexes, which provide a σ acceptor and a π donor orbital to form N<sub>2</sub> complexes (Figure 5c), singlet FB can be viewed as an electrophilic σ donor and π acceptor (Figure 5a). Its side-on attack on N<sub>2</sub> (Figures 5c and S12) enables electron donation from its sigma donor orbital into the π\* MO of N<sub>2</sub> and removal of π-bonding electrons into the π\* MO of BF. These bonding interactions are supported by an energy decomposition analysis (EDA).<sup>[22]</sup> This shows that the two major orbital interactions Δ*E*<sub>orb</sub>(1) and Δ*E*<sub>orb</sub>(2), which contribute with  $-119.3$  and  $-35.0$  kcal mol<sup>-1</sup> to the total orbital term Δ*E*<sub>orb</sub> in the transition state of the FB + N<sub>2</sub> reaction, can be attributed to σ(FB) donation and π(N<sub>2</sub>) back-donation, respectively (Figure S20). Since the reaction between boron and fluorine atoms is strongly exothermic (182 kcal mol<sup>-1</sup>),<sup>[20a]</sup> this reaction energy can provide the activation energy for the singlet FB + N<sub>2</sub> during the deposition of the matrix. It can, however, not be excluded that **C** can also be produced in an exothermic reaction of N<sub>2</sub> molecules with triplet excited FB (<sup>3</sup>Π), which is 80 kcal mol<sup>-1</sup> higher in energy than the singlet ground-state,<sup>[20a,c]</sup> and likely formed by UV radiation ( $\lambda < 357$  nm) emitted from the plasma plume.

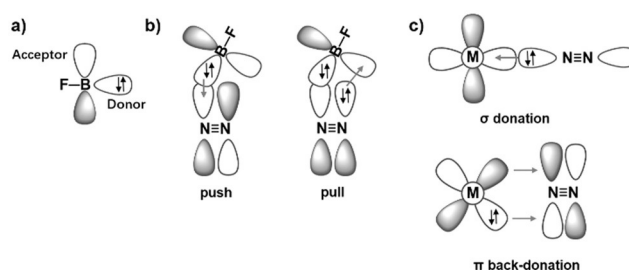


**Figure 5.** a) Scheme of the FB acceptor and donor orbitals. Note that FB has two mutually perpendicular π-acceptor orbitals, only one of which is shown. b) Bonding interaction in the transition state of the FB + N<sub>2</sub> reaction, c) end-on complex of N<sub>2</sub> to a transition metal M, see Figure S12.

We recall that **C** is observed only in freshly deposited samples, and it disappeared already upon annealing to 15 K. Cyclic **C** is isolectronic to the known diazirinone,  $\text{OC}(\eta^2\text{-N}_2)$ ,<sup>[23a]</sup> and although **C** should be more stable because of a higher barrier and a lower dissociation energy,<sup>[23b]</sup> the  $\text{N}=\text{N}$  bond in **C** is strongly activated and it reacts readily with a second singlet **FB** molecule to yield **A** through a very low energy barrier of  $0.5 \text{ kcal mol}^{-1}$  (Figure S5).

Since  $\text{B}_2\text{N}_2$  isomers were barely observed, they can hardly be considered as starting compounds for the bisfluoroborylene:  $\text{N}_2$  compounds **A** and **B**. However, **A** and **B** are most likely formed in an exothermic and low-barrier reaction from **BF** dimer molecules and  $\text{N}_2$  (Figure S5). The two lowest energy **BF** dimer isomers have been considered, the linear triplet  $\text{FB}=\text{BF}$  structure ( $^3\Sigma_g^-$ ) and a singlet *trans*-bent isomer of  $C_{2h}$  symmetry in a  $^1A_g$  ground state (Table S8). In contrast to the isolectronic **CO** dimer,  $\text{OCCO}$  ( $^3\Sigma_g^-$ ),<sup>[24]</sup> both of these **BF** dimers are more favourable than the diatomic fragments in their ground singlet state. The linear triplet **FBBF**, which formally arises from a double  $\sigma \rightarrow \pi^*$  excitation of the two singlet **BF** fragments,<sup>[8]</sup> is more stable than the *trans*-bent isomer by  $8 \text{ kcal mol}^{-1}$  (Table S8). On the other hand, the *trans*-bent isomer could be formed through mutual  $\sigma \rightarrow \pi$  donor-acceptor interactions of two ground-state singlet **BF** molecules via a loose and low-energy ( $< 1.0 \text{ kcal mol}^{-1}$ )  $C_{2h}$  symmetric transition state.<sup>[8]</sup> Since the computed anti-symmetric B-F stretching frequencies of these two isomers are similar (Table S8), our assignment of the experimentally observed B-F stretching frequencies to the *trans*-bent isomer (Table S8) is therefore very tentative and only supported by its predicted low-barrier formation from two singlet **BF** molecules. Nevertheless, the positive dissociation energy and the low barrier of formation of *trans*-bent **FBBF** from two **BF** molecules combined with a low barrier for the subsequent reaction with  $\text{N}_2$  molecules of  $10 \text{ kcal mol}^{-1}$  at the B3LYP/6-311++G(3df,3pd) level provide a surprisingly selective, low-barrier route to the title compound **A** on the singlet potential energy surface (Figure S5).

It was shown that the parent diborene,  $\text{HB}=\text{BH}$ , is efficiently stabilized by Lewis base ligands **L** to yield planar adducts  $\text{L}(\text{H})\text{B}=\text{B}(\text{H})\text{L}$ , with  $\text{L} = \text{CO}$ <sup>[25]</sup> or bulky carbene ligands.<sup>[26]</sup> Preliminary calculations at the B3LYP/6-311++g(3df,3pd) level indeed predict that also the addition of the weak  $\text{N}_2$  donor molecule to **FBBF** would be strongly exothermic and yield the corresponding adducts  $\text{FB}=\text{B}(\text{N}_2)\text{F}$  ( $C_s$ ,  $\Delta E = -25.6 \text{ kcal mol}^{-1}$ ) and  $\text{F}(\text{N}_2)\text{B}=\text{B}(\text{N}_2)\text{F}$  ( $C_{2h}$ ,  $\Delta E = -34.7 \text{ kcal mol}^{-1}$ , Table S9 and S10). However, we found no spectroscopic evidence for the predicted formation of these dinitrogen adducts of **FBBF** in the cryogenic  $\text{N}_2$ -matrix and we note that the adduct  $\text{FB}=\text{B}(\text{N}_2)\text{F}$  is still significantly higher in energy than the experimentally observed isomers **A** and **B** by 44 and 22  $\text{kcal mol}^{-1}$ , respectively. The cyclic compound **A** is both energetically (Figures S4, S5) and kinetically very stable, so that it can be expected that, like the analogous diazirinone,  $\text{OC}(\eta^2\text{-N}_2)$ ,<sup>[23a]</sup> it could be viable also at ambient conditions.

## Conclusion

In conclusion, the two novel cyclic fluorodiazaboririne,  $\text{FB}(\eta^2\text{-N}_2)$  (**C**), and 1,3-Diaza-2,4-diborete,  $(\text{FB})_2\text{N}_2$  (**A**), as well as the linear compounds  $\text{FB}=\text{BF}$  and **FBNBF** (**B**) were produced from laser-ablated boron atoms and fluorine embedded in an excess of  $\text{N}_2$ . The aromatic nature of the electron-deficient rings of **A** and **C**, reinforced by fluorine specific interactions based on electronic contribution from the  $\pi$  lone pairs of the exo-cyclic fluorine atoms, and confirmed by an MO analysis and computation of their NICS index, contributes to their high thermodynamic stability. Their surprisingly selective formation can be traced back to the high reactivity of fluoroborylene intermediates. This work may contribute to exciting applications in dinitrogen fixation and activation.

## Acknowledgements

We gratefully acknowledge financial support from the National Natural Science Foundation of China (nos. 21371136 and 21873070) and China Scholarship Council. Funded by the Deutsche Forschungsgemeinschaft (DFG, German Research Foundation)—Project-ID 387284271—SFB 1349. Open access funding enabled and organized by Projekt DEAL.

## Conflict of Interest

The authors declare no conflict of interest.

**Keywords:** aromaticity · dinitrogen activation · fluoroborylene · puckered  $\text{B}_2\text{N}_2$  ring

- [1] M. D. Fryzuk, *Acc. Chem. Res.* **2009**, *42*, 127–133.
- [2] a) T. N. Ye, S. W. Park, Y. F. Lu, J. Li, M. Sasase, M. Kitano, T. Tada, H. Hosono, *Nature* **2020**, *583*, 391–395; b) D. Singh, W. R. Buratto, J. F. Torres, L. J. Murray, *Chem. Rev.* **2020**, *120*, 5517–5581; c) J. K. F. Sebastian, S. Bastian, Y. Y. K. Ekaterina, S. Sven, *Chem. Rev.* **2021**, *121*, 6522–6587.
- [3] a) R. Kinjo, B. Donnadiou, M. A. Celik, G. Frenking, G. Bertrand, *Science* **2011**, *333*, 610–613; b) M. Soleilhavou, G. Bertrand, *Angew. Chem. Int. Ed.* **2017**, *56*, 10282–10292; *Angew. Chem.* **2017**, *129*, 10416–10426.
- [4] a) M. A. Légaré, G. Bélanger-Chabot, R. D. Dewhurst, E. Welz, I. Krummenacher, B. Engels, H. Braunschweig, *Science* **2018**, *359*, 896–900; b) M. A. Légaré, M. Rang, G. Bélanger-Chabot, J. I. Schweizer, I. Krummenacher, R. Bertermann, M. Arrowsmith, M. C. Holthausen, H. Braunschweig, *Science* **2019**, *363*, 1329–1332; c) H. Wang, L. L. Wu, Z. Y. Lin, Z. W. Xie, *Angew. Chem. Int. Ed.* **2018**, *57*, 8708–8713; *Angew. Chem.* **2018**, *130*, 8844–8849; d) M. A. Légaré, C. Pranckevicius, H. Braunschweig, *Chem. Rev.* **2019**, *119*, 8231–8261; e) K. Edel, M. Krieg, D. Grote, H. F. Bettinger, *J. Am. Chem. Soc.* **2017**, *139*, 15151–15159; f) M. J. Drance, J. D. Sears, A. M. Morse, C. E. Moore, A. L. Rheingold, M. L. Neidig, J. S. Figueroa, *Science* **2019**, *363*, 1203–1205; g) H. Braunschweig, R. D. Dewhurst, F. Hupp, M. Nutz, K. Radacki, C. W. Tate, A. Vargas, Q. Ye, *Nature* **2015**, *522*, 327–330.
- [5] D. C. Pestana, P. P. Power, *Inorg. Chem.* **1991**, *30*, 528–535.

- [6] a) P. Hassanzadeh, L. Andrews, *J. Phys. Chem.* **1992**, *96*, 9177–9182; b) L. Andrews, P. Hassanzadeh, T. R. Burkholder, *J. Chem. Phys.* **1993**, *98*, 922–931.
- [7] a) G. Deng, S. Pan, G. Wang, L. Zhao, M. Zhou, G. Frenking, *Chem. Eur. J.* **2021**, *27*, 2131–2137; b) G. Deng, S. Pan, J. Jin, G. Wang, L. Zhao, M. Zhou, G. Frenking, *Chem. Eur. J.* **2021**, *27*, 412–418.
- [8] A. A. Korkin, A. Balkova, R. J. Bartlett, R. J. Boyd, P. v. R. Schleyer, *J. Phys. Chem.* **1996**, *100*, 5702–5714.
- [9] a) B. Xu, L. Li, Z. Pu, W. J. Yu, W. J. Li, X. F. Wang, *Inorg. Chem.* **2019**, *58*, 2363–2371; b) B. Xu, W. J. Li, Z. Pu, W. J. Yu, T. F. Huang, J. J. Cheng, X. F. Wang, *Phys. Chem. Chem. Phys.* **2019**, *21*, 25577–25583; c) B. Xu, W. J. Li, W. J. Yu, Z. Pu, Z. Y. Tan, J. J. Cheng, X. F. Wang, L. Andrews, *Inorg. Chem.* **2019**, *58*, 13418–13425; d) X. F. Wang, B. O. Roos, L. Andrews, *Angew. Chem. Int. Ed.* **2010**, *49*, 157–160; *Angew. Chem.* **2010**, *122*, 161–164; e) X. F. Wang, L. Andrews, K. Willmann, F. Brosi, S. Riedel, *Angew. Chem. Int. Ed.* **2012**, *51*, 10628–10632; *Angew. Chem.* **2012**, *124*, 10780–10784; f) X. F. Wang, L. Andrews, F. Brosi, S. Riedel, *Chem. Eur. J.* **2013**, *19*, 1397–1409.
- [10] a) L. Xu, Q. Li, R. B. King, H. F. Schaefer, *Organometallics* **2011**, *30*, 5084–5087; b) L. Xu, Q. Li, R. B. King, *New J. Chem.* **2019**, *43*, 8220–8228.
- [11] M. F. Zhou, N. Tsumori, Z. H. Li, K. N. Fan, L. Andrews, Q. Xu, *J. Am. Chem. Soc.* **2002**, *124*, 12936–12937.
- [12] a) G. Maier, M. Naumann, H. P. Reisenauer, J. Eckwert, *Angew. Chem. Int. Ed. Engl.* **1996**, *35*, 1696–1697; *Angew. Chem.* **1996**, *108*, 1800–1801; b) Q. Liu, H. M. Li, Z. Wu, D. Q. Li, H. Beckers, G. Rauhut, X. Q. Zeng, *Chem. Asian J.* **2016**, *11*, 2953–2959.
- [13] K. A. Østby, G. Gundersen, A. Haaland, H. Nöth, *Dalton Trans.* **2005**, *13*, 2284–2291.
- [14] W. C. McKee, J. I. Wu, M. Hofmann, A. Berndt, P. v. R. Schleyer, *Org. Lett.* **2012**, *14*, 5712–5715.
- [15] T. Goswami, M. Homray, S. Paul, D. Bhattacharya, A. Misra, *Phys. Chem. Chem. Phys.* **2017**, *19*, 11744–11747.
- [16] A. T. Balaban, *Chem. Rev.* **2004**, *104*, 2777–2812.
- [17] J. C. Dobrowolski, P. F. J. Lipinski, *RSC Adv.* **2016**, *6*, 23900–23904.
- [18] NIST Chemistry WebBook, <http://webbook.nist.gov/chemistry/>.
- [19] a) A. Papakondylis, E. Miliordos, A. Mavridis, *J. Phys. Chem. A* **2004**, *108*, 4335–4340; b) J. M. L. Martin, P. R. Taylor, J. P. François, R. Gijbels, *Chem. Phys. Lett.* **1994**, *222*, 517–523.
- [20] a) F. Fantuzzi, T. M. Cardozo, M. A. C. Nascimento, *J. Phys. Chem. A* **2015**, *119*, 5335–5343; b) M. Lorenz, J. Agreiter, A. M. Smith, V. E. Bondybey, *J. Chem. Phys.* **1996**, *104*, 3143–3146; c) M. Krasowska, M. Edelmann, H. F. Bettinger, *J. Phys. Chem. A* **2016**, *120*, 6332–6341.
- [21] H. Zhang, R. Yuan, W. Wu, Y. Mo, *Chem. Eur. J.* **2020**, *26*, 2619–2625.
- [22] L. Zhao, M. V. Hopffgarten, D. M. Andrada, G. Frenking, *Wiley Interdiscip. Rev.: Comput. Mol. Sci.* **2018**, *8*, e1345.
- [23] a) X. Zeng, H. Beckers, H. Willner, J. F. Stanton, *Eur. J. Inorg. Chem.* **2012**, 3403–3409; b) H. Li, D. Li, X. Zeng, K. Liu, H. Beckers, H. F. Schaefer, B. J. Esselman, R. J. McMahon, *J. Phys. Chem. A* **2015**, *119*, 8903–8911.
- [24] J. Mato, D. Poole, M. S. Gordon, *J. Phys. Chem. A* **2020**, *124*, 8209–8222.
- [25] Z. Wang, Z. Chen, H. Jiao, P. v. R. Schleyer, *J. Theor. Comput. Chem.* **2005**, *4*, 669–688.
- [26] a) Y. Wang, B. Quillian, P. Wei, C. S. Wannere, Y. Xie, R. B. King, H. F. Schaefer, P. v. R. Schleyer, G. H. Robinson, *J. Am. Chem. Soc.* **2007**, *129*, 12412–12413; b) M. Arrowsmith, J. D. Mattock, J. Bohnke, I. Krummenacher, A. Vargasc, H. Braunschweig, *Chem. Commun.* **2018**, *54*, 4669–4672.
- [27] O. Parisel, M. Hanus, Y. Ellinger, *Chem. Phys.* **1996**, *212*, 331–351.

Manuscript received: May 25, 2021

Accepted manuscript online: June 11, 2021

Version of record online: June 26, 2021